Development of Low–Cost Air Quality Stations for Next Generation Monitoring Networks: Calibration and Validation of NO2 and O3 Sensors

Alice Cavaliere[1], Lorenzo Brilli[1], Bianca Patrizia Andreini[2,*], Federico Carotenuto[1], Beniamino Gioli[1], Tommaso Giordano[1], Marco Stefanelli[2,*], Carolina Vagnoli[1], Alessandro Zaldei[1], and Giovanni Gualtieri[1]

[1]National Research Council–Institute for BioEconomy (CNR–IBE), Via Caproni 8, 50145 Firenze, Italy
[2]ARPAT, Tuscany Region Environmental Protection Agency, Via Porpora, 22, 50144 Firenze, Italy
[*]These authors contributed equally to this work.

Correspondence: Alice Cavaliere (alice.cavaliere@ibe.cnr.it)

Abstract.

A Pre–deployment calibration and a field validation of two low–cost (LC) stations equipped with O3 and NO2 metal oxide sensors were addressed. Pre–deployment calibration was performed after developing and implementing a comprehensive calibration framework including several supervised learning models, such as univariate linear and non–linear algorithms, as well as multiple linear and non–linear algorithms. Univariate linear models included linear and robust regression, while univariate non–linear models included support vector machine, random forest, and gradient boosting. Multiple models consisted of both parametric and non–parametric algorithms. Internal temperature, relative humidity and gaseous interference compounds proved to be the most suitable predictors for multiple models, as they helped effectively mitigate the impact of environmental conditions and pollutant cross–sensitivity on sensor accuracy. A feature analysis, implementing Dominance analysis, feature permutations and, SHapley Additive exPlanations method, was also performed to provide further insight into the role played by each individual predictor and its impact on sensor performances. This study demonstrated that while multiple random forest (MRF) returned higher accuracy than multiple linear regression (MLR), it did not accurately represent physical models beyond the Pre–deployment calibration dataset, so that a linear approach may overall be a more suitable solution. Furthermore, as well as being less computationally demanding and generally more suitable for non–experts, parametric models such as MLR have a defined equation that also includes a few parameters, which allows easy adjustments for possible changes over time. Thus, drift correction or periodic automatable recalibration operations can be easily scheduled, which is particularly relevant for NO2 and O3 metal oxide sensors: as demonstrated in this study, they performed well with the same linear model form, but required unique parameter values due to inter–sensor variability.

1 Introduction

Low–cost (LC) air quality sensors are gaining more and more interest as they can provide near real–time observations with high spatial and temporal resolution. Their observations can be integrated into the current official regulatory networks, usually

monitoring air quality at lower space and time resolution, thus providing useful information to support policymakers and stakeholders in understanding air pollution dynamics (Brilli et al., 2021; Morawska et al., 2018). Dramatic advances in LC sensor technology have been made since their very first applications for monitoring CO, NO2 and NOx (De Vito et al., 2009),

25   O3 (Williams et al., 2013), and particulate matter (Holstius et al., 2014). Among gaseous species, NO2 and O3 are the most commonly investigated since both short– and long–term exposure to these pollutants are associated with higher risk to human health (Lin et al., 2018; Nuvolone et al., 2018; Meng et al., 2021; World Health Organization, 2021).

Typically, LC NO2 and O3 monitors use electrochemical (EC) or metal oxide sensors (MOS) (Narayana et al., 2022; Concas et al., 2021; Idrees and Zheng, 2020), which produce an analog signal proportional to pollutant concentration.

30   In their simplest configuration, EC sensors are based on a redox reaction within an electrochemical cell in which the target analyte oxidizes the anode or the cathode (Gäbel et al., 2022). As for MOS sensors, they have an exposed metal oxide surface film that changes its electrical properties when exposed to the target gas (Masson et al., 2015; Fine et al., 2010).

MOS sensors have a longer lifetime, can operate at higher temperatures and have a shorter response time and a wider operating range than EC sensors. By contrast, EC sensors have a lower power consumption as they do not require powering an

35   electric heater, and are less impacted by high humidity levels (Narayana et al., 2022; Concas et al., 2021).

Overall, to choose between MOS and EC sensors depends on the goals of the deployment. EC sensors should be preferred in areas with steady temperatures and weather conditions (Concas et al., 2021), while MOS sensors are more suited for long–term monitoring (Concas et al., 2021; Narayana et al., 2022; Burgués and Marco, 2018). LC sensors are affected by environmental factors such as air temperature and relative humidity (Barcelo-Ordinas et al., 2019; Mueller et al., 2017; Mead et al., 2013) and

40   suffer from cross–sensitivity with other air pollutants (Rai et al., 2017; Bart et al., 2014), thus complicating robust measurement recovery. These issues depend on sensor characteristics such as the type of electrolyte, electrode, or semiconductor material used (Spinelle et al., 2015). Unfortunately, the lack of information or inconsistency in data sheets from sensor manufacturers makes it challenging to accurately interpret the readings (Narayana et al., 2022). As a result, these issues must be addressed in the calibration process to ensure accuracy and reliability of LC field measurements.

45   Two main approaches to calibrating LC sensors exist (Spinelle et al., 2013): Pre–deployment and field calibration.

Pre–deployment calibration is typically performed in a controlled environment where LC sensors are exposed to a gas of known concentration in order to properly tune a calibration model (e.g., Claveau et al., 2022; Wei et al., 2018). Field calibration, on the other hand, consists in co–locating LC sensors near reference (official) stations that provide measured concentrations so as to develop a calibration model in real–world conditions (e.g., Spinelle et al., 2015). However, this approach may lead to

50   potential inaccuracies when the calibrated LC sensors are deployed on locations with varying air compositions and weather conditions (e.g., Spinelle et al., 2017; Aleixandre et al., 2013).

Both Pre–deployment and field calibration models are developed using a variety of mathematical methods, ranging from simple univariate regression models to more advanced machine learning techniques (Aula et al., 2022). The latter include various supervised learning techniques such as artificial neural networks (ANNs), random forest (RF), and support vector

55   regression (SVR) (e.g. Karagulian, 2023; Karagulian et al., 2019; Cordero et al., 2018). In addition, the use of covariates such as temperature and relative humidity, as well as interfering gasses as NO2, NO, and O3, can increase accuracy in the

calibration process Concas et al. (2021); Peterson et al. (2017); Piedrahita et al. (2014) . To date, while accuracy of LC calibration algorithms has been widely investigated, there is a lack of studies addressing crucial issues associated to these techniques, such as: (i) transferability of field calibration beyond the training range (as highlighted Nowack et al., 2021; Zauli–Sajani et al., 2021; De Vito et al., 2020; Esposito et al., 2018); (ii) Pre–deployment calibration complemented by a later field validation for EC and MOS sensors (as mentioned in Maag et al., 2018); (iii) the weight or importance of each feature included in multiple calibration models, particularly for black box techniques that cannot rely on statistical inference techniques (as mentioned in Sahu et al., 2021).

This study aims at addressing these issues by: (i) implementing a Pre–deployment calibration procedure for two LC stations measuring NO2 and O3 concentrations; (ii) identifying the optimal calibration that results in the highest accuracy; (iii) performing a long–term (more than 1–year) field validation against a regulatory station located in a different site; (iv) critically discussing transferability and scalability of the selected calibration model for multiple devices. These goals have been pursued by using ten among parametric, non–parametric univariate and multiple algorithms. Additionally, the investigation focused on delving deeper into the influence of internal temperature on LC sensors. To ensure comprehensive analysis, the covariate set for the multiple models was expanded to incorporate other essential factors such as humidity and gaseous interference compounds. Furthermore, the study utilized model–agnostic techniques, including SHapley Additive exPlanations (SHAP, Lundberg and Lee (2017)), to assess the model's generalization ability in a field environment. While SHAP has been employed in previous pollution–related studies (e.g., Wang et al., 2023; Chakraborty et al., 2022; Vega García and Aznarte, 2020), this research provides an original contribution by applying SHAP specifically to MOS sensors. This application aims to provide both local and global interpretations, resulting in a deeper understanding of the sensor's behaviour on individual data points and gaining insights into its overall performance.

2 Materials and Methods

2.1 AIRQino low–cost stations

The study focuses on two AIRQino LC air quality monitoring stations (hereinafter AQ) developed by the Institute for BioEconomy of the National Research Council of Italy (IBE–CNR) in Florence (Italy), namely AQ1 and AQ2, equipped with MOS sensors to measure O3 and NO2 concentrations (Zaldei et al., 2017; Di Lonardo et al., 2014). AQ consists of an Arduino Shield Compatible electronic board that integrates LC and high temporal resolution sensors (2–3 min data acquisition frequency) to monitor environmental parameters and atmospheric pollutants such as relative humidity, internal and external temperature, CO, CO2, O3, NO2, VOC, PM2.5, PM10. As for the atmospheric pollutants examined in this study (NO2 and O3), their concentrations are collected by SGX Sensortec MOS sensors: MiCS–2714 for NO2 (Sensortech, a) and MiCS–2614 for O3(Sensortech, b). These sensors consist of a micro metal oxide semiconductor diaphragm, with an integrated heating resistor (temperature ranges from 350 °C to 550 °C). The resistor–produced heat catalyses the reaction, which in turn affects the electrical resistance of the oxide layer itself. After the initial pre–heating period, the sensor detects gas changes in time intervals below 2 seconds. The output signal from the sensor is passed through an analog–to–digital converter (ADC) circuit with a 10 bit output. The

90 ADC converts the analog signal to a digital value between 0 and 1023 counts. This signal in counts is the primary output provided by the sensors (raw data). External air temperature (extT) and relative humidity (RH) are measured by an AM2305 (Asair) sensor protruding from the device enclosure. Internal temperature (intT) of the enclosure is monitored by a DS18B20 sensor (Maxim Integrated) that is mounted directly on the electronic board . Sensors' readings are collected by the onboard microprocessor and sent to a PostgreSQL database via a general packet radio service (GPRS) connection.

2.2   Reference instruments

During Pre–deployment calibration, reference pollutant concentrations were measured using two HORIBA instruments (HORIBA Ltd, Ambient Air Pollution AP SERIES analyzers). HORIBA model APNA–370 is an ambient nitrogen oxide monitor based on the chemiluminescence principle, allowing a continuous measurement of NO and NO2 concentrations. HORIBA model APOA–370 was used to collect O3 concentrations based on a cross flow modulated ultraviolet absorption method (Figure 1).
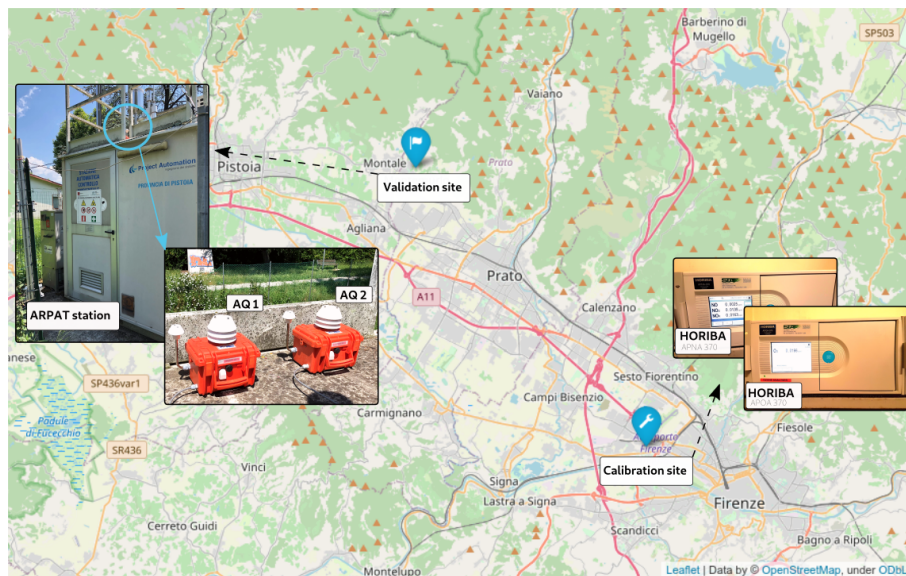

Figure 1. Map highlighting the calibration and validation locations for AQ1 and AQ2 LC air quality monitoring stations in Tuscany, Italy. At the calibration site (Florence), the HORIBA instruments used for calibrating the LC stations are shown, while at the validation site (Montale), the LC stations are pictured as installed on the roof of the reference ARPAT station (Air Quality Station EoI Code : IT1553A).

2.3   Sensor calibration

As detailed in Table S1 of the Supplementary material, Pre–deployment calibration of AQ1 and AQ2 stations against HORIBA analyzers was performed at CNR–IBE headquarters in Florence, Italy (43°47'52" N, 11°11' E, Figure 1). The AQ stations were mounted on a dedicated outdoor rack, while the HORIBA instruments were placed indoors in a laboratory setting. For outdoor air pollution sampling, approximately two–meter–long sampling probes were employed to collect outside air and channel it

4

directly to each of the reference instruments. HORIBA returned measurements at 3 min resolution collected across a 73 day period (19 July 2017–30 September 2017). To ensure data validity, measurements associated with RH>99 % following Wang et al. (2010) or classified as outliers by an interquartile range (IQR) method (Dekking et al., 2005) were removed from the dataset, eventually resulting in 58949 valid records for NO2, and 59261 valid records for O3 concentrations. The workflow of the Pre–deployment calibration process is shown in Figure 2.

Prior to implementing the calibration techniques, an exploratory data analysis (EDA) was conducted using the correlation matrix to identify important insights. The study further explored the potential generalizability of the relationship between MOS O3 sensors and temperature, as highlighted in Spinelle et al. (2016), leveraging observations from the correlation matrix. The core of the calibration framework consisted of a set of supervised learning algorithms previously evaluated in the literature, falling in two categories: univariate and multiple models. The former are based on a single predictor (pollutant raw data), while the latter include additional predictors. Both categories included linear and non–linear algorithms. During the training phase, the datasets containing both LC and reference measurements were divided into a training subset consisting of 67 % of the data and a testing subset consisting of the remaining 33 %.

The suite of algorithms for univariate calibration linear methods included linear regression (Mijling et al., 2018; Maag et al., 2016) and robust regressions (Cavaliere et al., 2018) while the non–linear approaches comprised support vector machine (Bigi et al., 2018; Gu et al., 2018), random forest (Han et al., 2021; Zimmerman et al., 2018) and gradient boosting (Lin et al., 2018; Johnson et al., 2018). Multiple models, which considered temperature, humidity, and cross–sensitivity parameters for prediction, consisted of both parametric models and non–parametric models (Gäbel et al., 2022; Sayahi et al., 2020; Spinelle et al., 2017).

2.3.1 Univariate models

The suite of univariate algorithms included a total of ten models, falling in three main categories: (i) linear regression (SLR), (ii) non–linear regression (SNLR), and (iii) support vector machine (SVM). Five regression models are included in SLR: simple linear regression (LR); polynomial regression of second (PLR2) and third (PLR3) degree; Huber regression (HBLR), a robust regression technique to outliers that uses a different loss function rather than the traditional least–squares; and Cook's distance regression (CDLR, Cook (1977)) which summarizes how much all values in the regression model change when the i–th observation is removed. Non–linear regression (SNLR) included parametric and non–parametric models. The former included power non–linear regression (PNLR) and logarithm regression (LNLR), which considers the estimation of coefficients through the Levenberg–Marquardt algorithm. The latter included Random Forest (RF) and Gradient Boosting (GB). Random Forest conducts optimal splitting of data samples into smaller sample sets, which then are fitted respectively along the tree paths, while Gradient Boosting built an additive model based on gradient boosting decision trees and in each stage a regression tree was fit. In the present calibration, the RF model used the mean square error as a fitting function in order to evaluate each decision split. Finally SVM included support vector regression using linear kernel (SVR) and radial basis function (RBF). In SVM, the kernel allows to identify a hyperplane with maximum margin such that the maximum number of data points are within that margin.
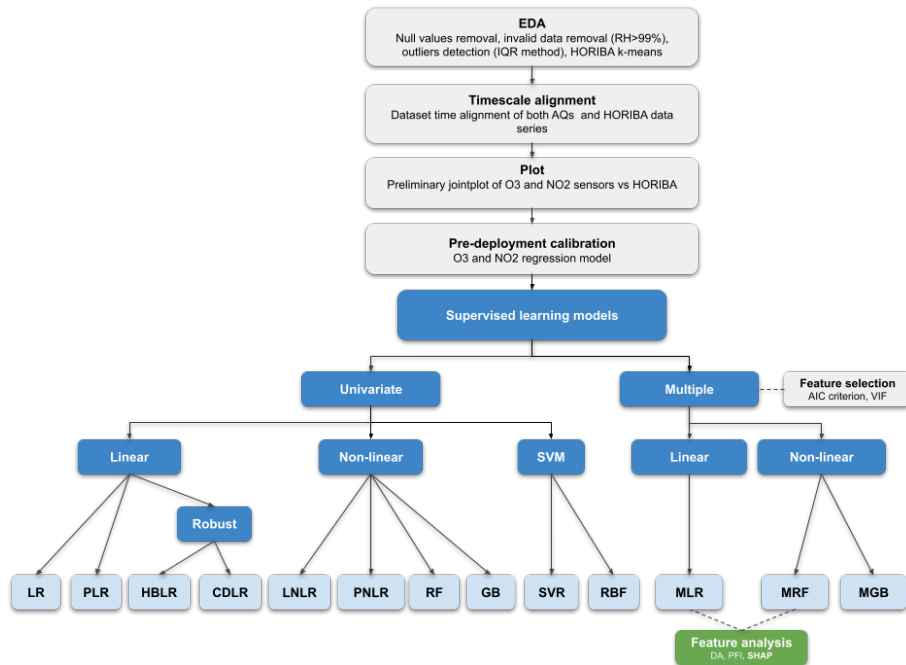
Figure 2. Workflow of the Pre–deployment calibration process performed in the work. The model abbreviations are also listed in the Appendix as Table A1.

For each non–parametric models the grid search method was used to optimize the default hyper parameter values (Pedregosa et al., 2011; Smets et al., 2007).

2.3.2 Multiple models

Multiple models included both linear (MLR) and non–linear models, the latter consisting of multiple random forest (MRF) and multiple gradient boosting (MGB). While implementing an MLR model, a linear stepwise multi–regression analysis was carried out by automatically generating all possible models starting from a list of explanatory variables. In the case of NO2 and O3 sensors, the latter included internal temperature (intT), external temperature (extT) and relative humidity (RH). In order to solely include statistically significant variables, thus excluding possible collinearity between them, the variance inflation factors (VIFs) were examined for each generated model. To refine the choice between internal and external temperature, a multiple linear model was used that alternatively incorporated both temperatures, followed by a cross–validation. Once a subset of significant explanatory variables was identified during multiple linear regresison (MLR) implementation, the multiple Random Forest (MRF) and multiple Gradient Boosting (MGB) models were also applied: MGB was selected as Gradient Boosting is the univariate model that improves the results obtained by the supervised machine learning model, while MRF was selected as being a model widely used in the literature (e.g., Bisignano et al., 2022; Bigi et al., 2018; Zimmerman et al., 2018). To compare

the performance between models, specified metrics were evaluated such as the adjusted R–squared (AdjR^2, Draper and Smith (1998)). In Table S2, a concise summary of the initialization hyperparameters applied to the models is provided.

2.3.3 Multiple models interpretation

To gain a better understanding of the impact due to different predictors and an insightful interpretation of the multiple model results, several analysis techniques have been applied, such as permutation feature importance (PFI, Breiman (2001)), dominance analysis (DA, Azen and Budescu (2003)), and SHapley Additive exPlanations (SHAP, Lundberg and Lee (2017)) analysis.

PFI is a model inspection technique that measures the global variable importance by observing the effect of randomly shuffling each explanatory variable. DA is a common procedure for identifying the relative importance of predictors in a linear model. In this work, five different DA statistics were evaluated: (i) interactional dominance (IntD); (ii) individual dominance (ID); (iii) average partial dominance (APD); (iv) total dominance (TD); (v) percentage relative importance (PRI).

SHAP analysis is a model–agnostic approach based on the game theory that can be applied to any machine learning model as a post hoc interpretation technique. According to the SHAP analysis, each machine learning model's prediction, $f(x)$, can be represented as the sum of its computed SHAP values, plus a fixed base value, as shown in Eq. (1):

$$f(x) = \Phi_0 + \sum_{i=1}^{p} \Phi_i \tag{1}$$

where Φ_0 is the base value of the model, which represents the average prediction across all inputs, and Φ_i is the SHAP value for feature i for the input x. Each Φ_i is computed as Eq. (2):

$$\Phi_i = \sum_{S \subseteq 1,2,\ldots,p \setminus i} \frac{(p - |S| - 1)! \cdot |S|!}{p!} \cdot [f(x_{S \cup i}) - f(x_S)] \tag{2}$$

where p is the total number of features, S is a subset of all features except for feature i, $|S|$ is the number of features in subset S, $f(x_S)$ is the model's prediction for input x with features in subset S, and $f(x_{S \cup i})$ is the model's prediction for input x with features in subset S and feature i included.

SHAP values are calculated for each feature and value present in the dataset, and they approximate the contribution towards the output given by that data point. To compute SHAP values for different types of machine learning models, various SHAP implementations are available. In this study, the SHAP Linear Explainer function was used for MLR predictors, while the FastTreeSHAP explainer (Yang, 2021) was used for other models. Compared to the widely used TreeSHAP algorithm, FastTreeSHAP provides faster computation of feature importance values for tree–based models.

2.4 Field validation

To test Pre–deployment calibration models, the AQ stations were subject to a field validation based on hourly measurements collected during 429 consecutive days (19 June 2018–22 August 2019) by a reference air quality station operated by the

Tuscany Region Environmental Protection Agency (ARPAT). High resolution NO2 and O3 concentrations measured by the AQ stations over the same period were hourly averaged in order to be aligned to the reference data . Overall, datasets of valid hourly records ranging 7383–9340 for NO2, and 7344–9303 for O3 concentrations, were used (Table S1). The reference air quality station (EoI Code : IT1553A) was located at Montale, a small town in Tuscany located between the cities of Prato and Pistoia (43°54'57" N, 11°00'26" E), and classified as a suburban background station (Figure 1). The ARPAT reference station and the HORIBA APNA–370 analyzer used the same method for measuring NO2, while a different method (ultraviolet photometry) was used by ARPAT to measure O3.

2.5 Statistics and libraries

The performances of each AQ station during both Pre–deployment calibration and field validation were computed using various statistical measures, including Pearson correlation coefficient (r), coefficient of determination (R^2), adjusted R–squared (AdjR^2), root mean squared error (RMSE), normalized RMSE (nRMSE), which takes into account the range of values by dividing the RMSE by the difference between the maximum and minimum values, mean absolute error (MAE), and mean bias error (MBE). Variance impact factor (VIF) and Akaike information criterion (AIC) were also applied to discriminate between MLR models. All calculations related to calibration procedure and analysis of performance of calibrated units are implemented using Python Sklearn library (Pedregosa et al., 2011) and Python statsmodels module (Seabold and Perktold, 2010). Finally, feature evaluation of MLR and MRF models was performed using python Dominance–Analysis library (Shekhar et al., 2019), SHAP library (Lundberg and Lee, 2022), FastTreeSHAP library (Yang, 2022), and ELI5 Permutation Importance library (TeamHG-Memex, 2022).

3 Results

3.1 Exploratory data analysis

After applying the humidity threshold and IQR procedure, 2 % and 12 % of records were withdrawn from the initial datasets of AQ1 and AQ2 stations, respectively. The comparison between the resulting O3 and NO2 data and the HORIBA reference concentrations is shown in Figure 3. Based on the analysis of Pearson's correlation (Fig. S3), three patterns for both AQ stations emerged as conforming to the existing literature. HORIBA NO2 and O3 had a negative Pearson's r (r_{AQ1}=-0.77, r_{AQ2}=-0.75), compatible with the chemical coupling of O3 and NOx=NO+NO2 (Han et al., 2011). AQ intT had a high positive correlation with HORIBA O3 (r_{AQ1}=0.79, r_{AQ2}=0.80) compatible with the fact that high temperatures can increase the rate of O3 formation through photochemical reactions (Han et al., 2011). AQ RH had a high negative correlation with HORIBA O3 (r_{AQ1}=-0.75,r_{AQ2}=-0.74), compatible with the fact that high relative humidity is generally associated with lower O3 levels (Camalier et al., 2007). Moreover, as a result of the convective heat transfer equation, a strong positive correlation was observed between intT and extT for each AQ ($r_{AQ1,AQ2}$=1). On average, the temperature difference between intT and extT remains relatively constant at around 8 °C. A visual representation of the difference between the two temperatures, plotted

against their mean, can be found in the Bland–Altman plots on Figure S4. No significant correlation was observed between NO2 raw and either temperature or RH. Moderate positive associations were instead found between O3 raw and both intT (r_{AQ1}=0.55; r_{AQ2}=0.55) and extT (r_{AQ1}=0.52; r_{AQ2}=0.53).
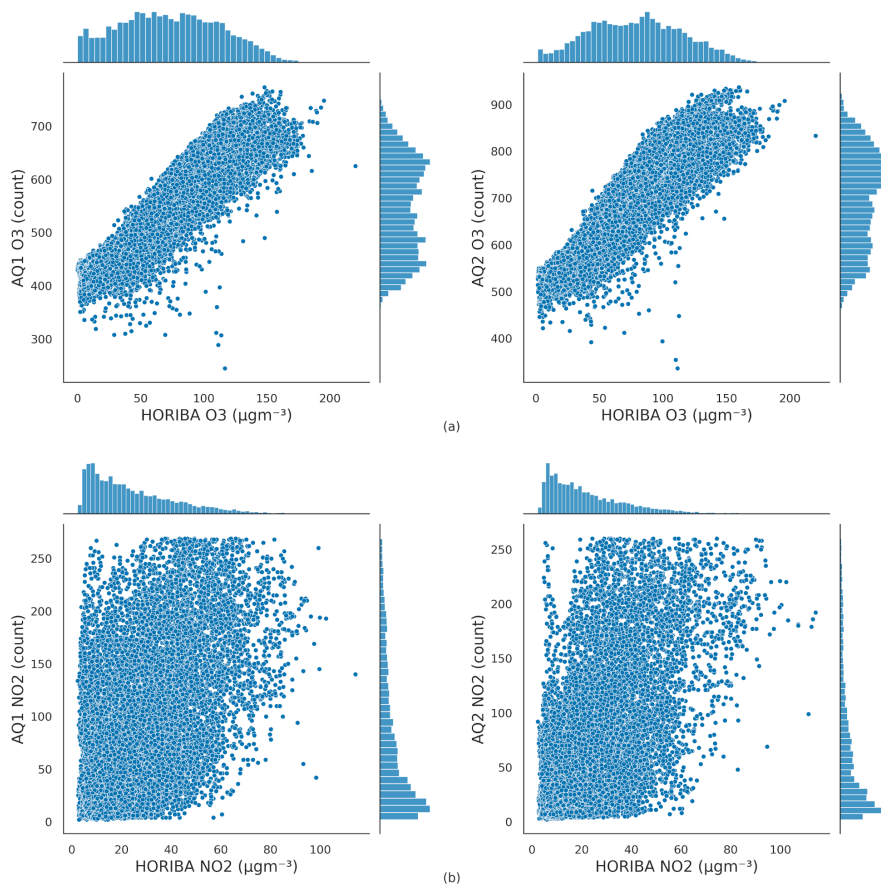

Figure 3. Scatter Plots of 3 min sampled AQ1 and AQ2 signals vs. HORIBA reference concentrations observed during Pre–deployment calibration: O3(a); NO2(b).

3.2 Univariate models

215 The results of the supervised linear (SLR), supervised non–linear (SNLR) and support vector machine (SVM) models applied for both AQ stations and pollutants are reported in Table 1. For both AQ stations, the best performances were found using the GB model, with O3 concentrations generally better fitted than NO2 concentrations.

Table 1. Table 1. Statistics of the univariate regression models applied to the AQ1 and AQ2 stations. Note that for non–linear models (LNLR and PNLR) R^2 is not a useful metric, while it is for linear models that use polynomials to model curvature in the data (Spiess and Neumeyer, 2010)

Pollutant	AQ id	Stat.	SLR					SNLR				SVM	
			LR	PLR2	PLR3	CDLR	HBLR	LNLR	PNLR	RF	GB	SVR	RBF
O3	AQ1	R^2	0.81	0.81	0.82	0.81	0.81	0.00	–	0.82	0.82	0.81	0.70
		RMSE	16.92	16.92	16.75	16.99	17.00	17.15	18.85	16.78	16.58	17.18	21.31
		MAE	13.42	13.41	13.40	13.19	13.18	13.47	14.94	13.42	13.27	13.12	16.06
		MBE	-0.28	-0.28	-0.30	1.56	1.69	-0.33	-0.96	-0.18	-0.20	2.89	3.53
	AQ2	R^2	0.77	0.77	0.77	0.76	0.77	–	–	0.77	0.78	0.76	0.60
		RMSE	17.58	17.55	17.41	17.86	17.75	17.97	18.46	17.58	17.36	18.11	23.06
		MAE	14.11	14.10	14.10	13.81	13.85	14.30	14.79	14.18	14.05	13.79	17.38
		MBE	0.14	0.14	0.15	3.03	2.39	0.19	-0.48	0.24	0.14	4.17	3.55
NO2	AQ1	R^2	0.34	0.34	0.34	0.32	0.33	–	–	0.33	0.35	0.33	0.31
		RMSE	14.22	14.18	14.16	14.40	14.28	14.51	14.46	14.35	14.14	14.35	14.50
		MAE	10.91	10.84	10.82	10.77	10.79	11.20	11.22	10.84	10.75	10.76	10.81
		MBE	0.09	0.11	0.11	2.26	1.21	0.16	-0.11	0.06	0.09	1.73	2.08
	AQ2	R^2	0.38	0.38	0.38	0.35	0.37	–	–	0.36	0.38	0.36	0.32
		RMSE	12.86	12.85	12.85	13.12	12.95	13.45	13.06	13.04	12.85	13.02	13.39
		MAE	9.83	9.83	9.84	9.69	9.69	10.37	10.06	9.94	9.81	9.67	9.83
		MBE	-0.09	-0.09	-0.09	2.56	1.53	-0.05	-0.24	-0.05	-0.10	2.05	2.60

3.3 Multiple regression

EDA suggested that the inclusion in multiple regression models of both intT and extT may result in unstable results due to their
220 strong collinearity ($r_{AQ1,AQ2}$=1). This was confirmed by the variance inflation factor (VIF) for the MLR model, which was higher than 5 when both variables were used (Table S5). To ensure consistent selection of the optimal temperature variable in the model, cross–validation procedure was conducted on the calibration dataset for the MLR model, alternately including intT

and extT in the covariate set. The results of 5–split cross–validation (Table 2) showed no significant differences using intT or extT, whilst the use of intT provided a slightly higher mean accuracy and a lower mean RMSE.

Table 2. R^2 and RMSE (μgm^{-3}) values by covariate set including intT or extT variables of the cross–validation procedure applied to the MLR model.

			Covariate set (mean±SD)	
AQ id	Pollutant	Stat.	O3,NO2,intT,RH	O3,NO2,extT,RH
AQ1	O3	R^2	0.93±0.03	0.93±0.02
		RMSE	9.52±2.51	9.55±2.10
AQ2	O3	R^2	0.91±0.04	0.91±0.05
		RMSE	9.52±2.86	9.72±2.85
AQ1	NO2	R^2	0.57±0.21	0.56±0.24
		RMSE	10.75±1.31	10.83±1.43
AQ2	NO2	R^2	0.61±0.07	0.61±0.07
		RMSE	9.87±2.07	9.89±2.02

225   Following the previous result, the final subset of predictors used for all models consisted of intT, RH, and raw signal from both sensors (Tables S6 and S7). Accordingly, for both stations, Eq.3 and Eq.4 were the best model formulas for O3 and NO2 sensors, respectively:

$$O_3 = \beta_0 + \beta_1 \cdot NO_2raw + \beta_2 \cdot O_3raw + \beta_3 \cdot RH + \beta_4 \cdot intT \tag{3}$$

$$NO_2 = \beta_0 + \beta_1 \cdot NO_2raw + \beta_2 \cdot O_3raw + \beta_3 \cdot RH + \beta_4 \cdot intT \tag{4}$$

230   The calibration coefficients achieved for the MLR model are reported in Table 3, while the scores of MLR, MGB and MRF model application are reported in Table 4.

Table 3. Statistics of the MLR model applied to the AQ1 and AQ2 stations. β_0 are the intercepts and β_i the calibration coefficients.

		Coefficient					Stat.
Pollutant	AQ id	$\beta 0$	$\beta 1$	$\beta 2$	$\beta 3$	$\beta 4$	AdjR^2
O3	AQ1	-180.76	-0.11	0.23	0.15	3.79	0.95
	AQ2	-133.43	-0.16	0.14	0.03	3.58	0.95
NO2	AQ1	144.78	0.05	-0.14	-0.32	-0.93	0.69
	AQ2	126.78	0.08	-0.10	-0.23	-0.87	0.69

Overall, O3 concentrations were better fitted than NO2 concentrations, while MRF proved to be the finest model, generally outperforming MGB and particularly MLR model.

Table 4. Statistics of the multiple regression models applied to the AQ1 and AQ2 stations.

Pollutant	AQ id	Stat.	Multiple models		
			MLR	MGB	MRF
O3	AQ1	$AdjR^2$	0.95	0.97	0.98
		RMSE	8.62	7.30	6.04
		MAE	6.30	5.40	4.31
		MBE	-0.10	-0.01	-0.01
	AQ2	$AdjR^2$	0.95	0.96	0.98
		RMSE	8.58	6.86	5.51
		MAE	6.50	5.17	4.05
		MBE	-0.03	-0.03	0.09
NO2	AQ1	$AdjR^2$	0.69	0.80	0.86
		RMSE	9.68	7.84	6.63
		MAE	7.36	5.76	4.72
		MBE	-0.03	0.06	0.06
	AQ2	$AdjR^2$	0.69	0.80	0.85
		RMSE	9.07	7.28	6.30
		MAE	6.83	5.35	4.46
		MBE	-0.08	0.03	0.05

3.4 Multiple models interpretation

In terms of traditional statistical inference techniques such as DA and PFI during MLR and MRF O3 calibration, the results primarily confirmed O3 raw and secondly intT as the most significant predictors (Table 5), which were consistent with those reported by Masson et al. (2015). Overall, the DA analysis showed that O3 raw and intT were the most important features for both stations and pollutants. In particular, for O3 concentrations O3 raw data resulted in the highest PRI value, explaining 38.96 % and 34.95 % of the R^2 of the MLR model for AQ1 and AQ2, respectively, followed by intT (28.64 % and 31.51 %, respectively). Also for NO2 concentrations, O3 raw data had the highest PRI value, explaining 55.18–51.13 % of the R^2 of the MLR model, followed by NO2 raw data (23.78–26.79 %). In O3 MRF regression, O3 raw was the most important feature for AQ1, while it was intT for AQ2. Conversely, in NO2 MRF regression, O3 raw was the most important feature for both AQ stations followed by RH for AQ1 and by NO2 for AQ2. Notably, for both MLR and MRF models, O3 raw proved to be a more important feature in NO2 calibration than in O3 calibration.

Table 5. DA statistics and PFI weights achieved for MLR and MRF models applied to the AQ1 and AQ2 stations.

Pollutant	AQ id	Variable	IntD	ID	DA APD	TD	PRI	PFI Weight
O3	AQ1	O3	0.09	0.82	0.29	0.37	38.96	0.66 ± 0.01
		intT	0.07	0.62	0.20	0.27	28.64	0.48 ± 0.01
		RH	0.00	0.57	0.10	0.19	19.92	0.01 ± 0.00
		NO2	0.02	0.26	0.10	0.12	12.47	0.16 ± 0.01
	AQ2	O3	0.06	0.77	0.25	0.33	34.95	0.47 ± 0.01
		intT	0.11	0.64	0.22	0.30	31.51	0.55 ± 0.01
		RH	0.00	0.55	0.09	0.18	19.10	0.01 ± 0.00
		NO2	0.03	0.31	0.10	0.14	14.44	0.20 ± 0.01
NO2	AQ1	O3	0.16	0.66	0.36	0.39	55.18	1.12 ± 0.02
		NO2	0.02	0.34	0.15	0.17	23.78	0.21 ± 0.01
		intT	0.02	0.20	0.06	0.08	11.93	0.18 ± 0.01
		RH	0.03	0.18	0.02	0.06	9.11	0.22 ± 0.01
	AQ2	O3	0.12	0.64	0.33	0.35	51.13	1.01 ± 0.04
		NO2	0.04	0.38	0.16	0.19	26.79	0.19 ± 0.01
		intT	0.03	0.21	0.06	0.09	13.34	0.18 ± 0.01
		RH	0.03	0.18	0.02	0.06	8.74	0.16 ± 0.01

The challenge with traditional feature selection methods like DA and PFI is that they may produce misleading results when features are highly correlated or the data is noisy. These methods in fact do not consider interactions or correlations between

predictors, and DA is only applicable to linear models. To overcome these limitations, the study utilized SHAP analysis. The SHAP analysis was performed in order to gain insight into both global and local contribution of each feature at both individual instance level and across the population, resulting in the SHAP bee swarm plots for MLR and MRF shown in Figures **??** and 4, respectively. The bee swarm plot ranks the input features from the highest to the lowest mean absolute SHAP values for the entire dataset. For each variable, every instance of the dataset appears as its own point. The points are distributed horizontally along the x–axis according to their SHAP value. In places where there is a high density of SHAP values, the points are stacked vertically. The color bar corresponds to the raw values of each feature for each instance, providing a visual representation of the feature's contribution to the outcome prediction.
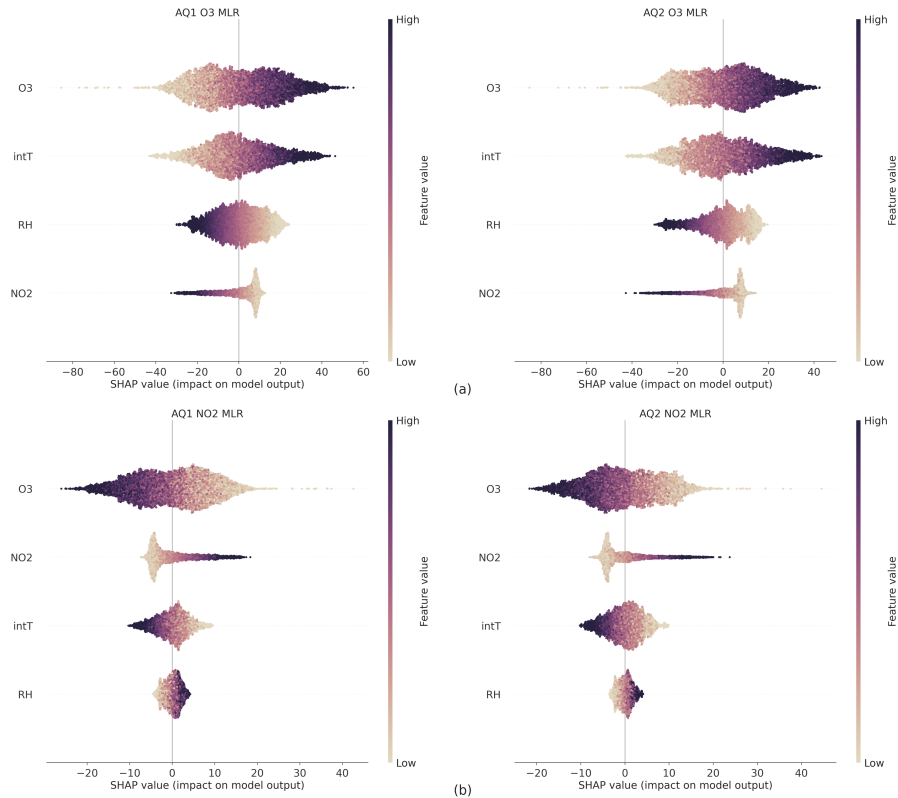

Figure 4. Bee swarm plot showing the SHAP values calculated for each feature and instance using the linear explainer the MLR model for O3 (a) and NO2 (b).
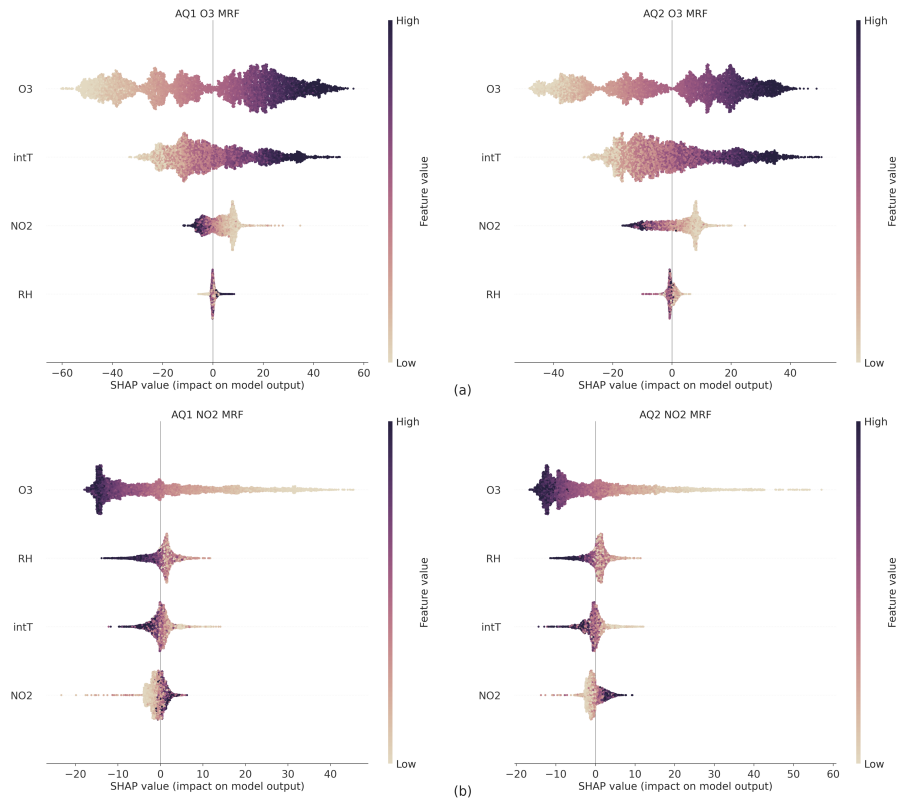
Figure 5. Bee swarm plot showing the SHAP values calculated for each feature and instance using the fast tree explainer of the MRF model for O3 (a) and NO2 (b).

As for the MLR model for both AQ stations, high levels of both O3 raw and intT data had a strong and positive impact on O3 output, as indicated by high and positive SHAP values (Fig. 4a), while high levels of NO2 raw data had a strong and positive impact on NO2 output (Figure 4b). Herein, however, high levels of O3 raw and intT data had a greater impact on decreasing the predicted values of NO2 than the raw data of NO2.

Also for the MRF model O3 raw data had a high influence on O3 predicted values (Fig. 6a): higher values of O3 raw data increased O3 prediction, while lower values had a negative effect. This also applies to the NO2 output values (Fig. 6b), as higher values of O3 raw data decreased NO2 prediction and lower values had a positive effect. Herein, however, high or low levels of NO2 raw had no significant influence on the prediction.The mean absolute SHAP values for all features of both MLR and MRF models are reported in Figure S8.

In order to provide a local interpretability, a heatmap for the SHAP values of the NO2 MLR model was also elaborated (Figure 6). The heatmap showed that lower model predictions $f(x)$, computed using Eq.(1), were linked to a dark colour for O3 and a light colour for NO2 for both AQs. This suggested that O3 raw data had a more significant impact mostly on the lower NO2 concentrations than NO2 raw itself had while the impact of NO2 raw data became significant at higher concentrations.
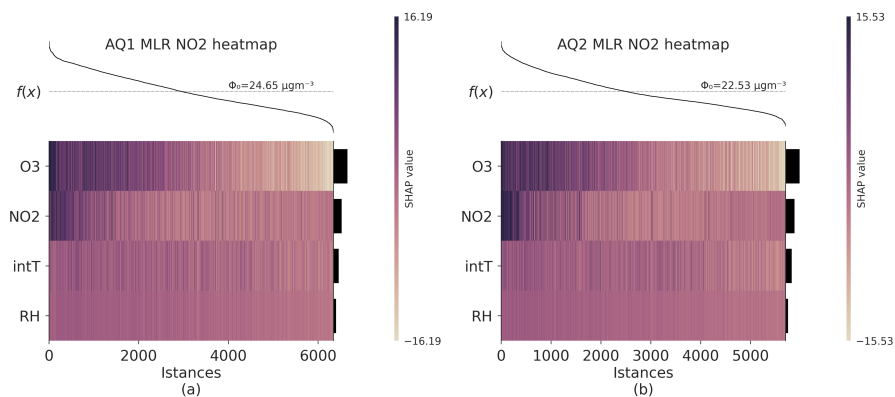

Figure 6. Heatmap of SHAP values of the NO2 MLR model for AQ1 (a) and AQ2 (b). The heatmap displays the contribution of each feature to the model's predictions, with positive contributions represented by dark–colored cells cells and negative contributions by light–colored cells. Colour intensity denotes the magnitude of the contribution. The output of the model, $f(x)$, is shown above the heatmap matrix, centred around the explanation's base value (ϕ_0), and the global importance of each model input is shown in the bar plot on the right–hand side of the plot. Observations have been ordered by the sum of the SHAP values over all features.

3.5 Field validation

The scores of field validation involving the MLR and MRF calibrated models are summarized in Table 6. Model accuracy in
270 predicting O3 concentrations is confirmed to be higher than in predicting NO2 concentrations. In terms of Pearson's r values,
the MLR model outperforms the MRF model, as exhibiting r values (0.92–0.93 for O3 and 0.75–0.78 for NO2) higher than
MRF (0.81–0.76 for O3 and 0.76–0.65 for NO2), while the opposite applies in terms of standard deviation, as MRF returns
lower values than MLR. Notably, a significant difference by AQ station may be observed in MRF scores, while it is not the
case for MLR.
275 Taylor diagrams of the pre–deployment MLR and MRF calibrated models assessed against the ARPAT reference station for
O3 (a) and NO2 (b) concentrations may be found in Figure S10, while weekly concentrations predicted by the models against
the reference station are given in Figure 7.

Table 6. Statistics of the MLR and MRF calibrated models assessed during the field validation procedure.

Pollutant	AQ id	Stat.	MLR	MRF
O3	AQ1	r	0.92	0.81
		CRMSD	15.98	24.13
		RMSE	16.52	29.08
		MAE	12.96	22.22
		MBE	4.20	16.23
	AQ2	r	0.93	0.76
		CRMSD	15.35	25.44
		RMSE	17.88	42.98
		MAE	13.99	36.24
		MBE	9.17	34.64
NO2	AQ1	r	0.75	0.65
		CRMSD	11.25	11.83
		RMSE	12.64	13.48
		MAE	9.40	9.97
		MBE	5.75	6.46
	AQ2	r	0.78	0.58
		CRMSD	10.63	11.77
		RMSE	10.65	11.94
		MAE	7.72	9.12
		MBE	–0.69	2.03

Figure 7. Trend analysis of 7–day average O3 and NO2 concentrations measured at the validation site by the calibrated AQ1 and AQ2 stations compared to the ARPAT reference station (17 June 2019–22 August 2019)

A seasonal analysis was also performed for MLR field validation (Table 7). O3 concentrations were well predicted across all seasons: for both stations, the lowest nRMSE values were registered in the summers 2018 and 2019, and the highest in winter 2018–2019. Notably, all statistical scores during the summer 2019 proved to be worse compared to the summer 2018, suggesting a likely drift in sensor accuracy after one year of deployment. As for NO2, the highest (and thus more meaningful) concentrations were measured in winter 2018–2019. The NO2 scores during this period, however, confirm to be worse than those affecting O3 during the period of highest O3 concentrations (i.e. summers 2018 and 2019). Furthermore, the scores of seasonal analysis addressed for MRF field validation may be found in Table S12.

Table 7. Seasonal analysis of MLR validation. Min–Max ($\mu\mathrm{gm}^{-3}$) represent the minimum and maximum concentrations measured by the reference station, while intT (°C) the average internal temperature measured by the AQ stations.

Year	Season	Pollutant	AQ id	min–max	intT	r	nRMSE	MAE	MBE
							Stat.		
2018	Summer	O3	AQ1	6–166	34.65	0.94	9.17	11.69	-5.17
			AQ2	6–166	34.20	0.94	8.80	11.07	7.57
		NO2	AQ1	1–47	34.62	0.69	35.74	14.04	13.83
			AQ2	1–47	34.16	0.69	16.97	5.94	2.90
	Autumn	O3	AQ1	2–146	28.06	0.93	13.24	15.08	11.35
			AQ2	2–146	25.53	0.94	15.87	19.32	18.37
		NO2	AQ1	1–62	28.07	0.73	19.66	8.62	5.57
			AQ2	1–62	25.54	0.71	16.57	7.60	-2.40
	Winter	O3	AQ1	2–65	16.60	0.93	17.94	8.07	0.11
			AQ2	2–72	14.53	0.93	18.97	8.97	2.50
		NO2	AQ1	3–88	16.59	0.71	21.01	13.97	10.44
			AQ2	2–88	14.53	0.70	18.34	12.16	4.62
2019	Spring	O3	AQ1	2–132	22.41	0.86	13.32	13.98	3.36
			AQ2	2–132	21.14	0.84	13.91	14.40	4.63
		NO2	AQ1	2–63	22.32	0.74	13.18	6.10	-2.09
			AQ2	2–63	21.09	0.67	16.19	7.31	-5.36
	Summer	O3	AQ1	7–185	34.98	0.92	10.09	14.62	10.21
			AQ2	7–185	32.29	0.92	10.68	15.98	12.71
		NO2	AQ1	0–47	34.94	0.63	17.82	6.36	3.58
			AQ2	0–47	32.25	0.68	13.68	5.01	-3.05

4 Discussion

Current outcomes achieved for MOS O3 and NO2 pre–deployment calibration were generally consistent with those found in the literature. MOS NO2 calibration exhibited low accuracy in linear univariate models, as demonstrated by Nowack et al. (2021), and the MiCS–2710 NO2 sensor achieves a poor R^2 (0.21) compared to the O3_3E1F EC sensor's value (0.845), as reported by Spinelle et al. (2015). In contrast, O3 sensor calibration returns high R^2 values, suggesting limited potential for improvement using more complex univariate techniques like SVR, RF, or GB, as noted in Sales-Lérida et al. (2021). For NO2 calibration, incorporating multiple covariates like temperature, humidity, and gaseous interference compounds was instead essential for better performance, as emphasized in studies cited in Karagulian et al. (2019).

This study confirmed that both linear and non–linear multiple models resulted in a slight improvement in O3 calibration and a significant one in NO2 prediction compared to univariate models (Table 4). In particular, the MLR model improved the accuracy of the simple LR by more than 14–18 % for O3 and 31–35 % for NO2. Notably, both MOS sensors performed well using the same model form, but due to inter–sensor variability, each sensor necessitated a distinct set of coefficients to achieve optimal performance. Moreover, taking into account the observed multicollinearity issue between temperatures and the slightly higher mean accuracy, as well as the lower mean RMSE observed when using the internal one (Table 2), the study drew upon insights from existing literature to identify the most suitable set of covariates (e.g., Miech et al., 2021; Schmitz et al., 2021). As a result, the inclusion of internal temperature as a significant factor was given priority, as it offers a more accurate representation of the operating conditions of the MOSs within the system. This approach was also adopted to tackle potential challenges in the board's analog–to–digital converter circuit.

However among the multiple models, MRF proved to be the most effective in the pre–deployment calibration (e.g., Bisignano et al., 2022; Johnson et al., 2018). The SHAP methodology proved to be particularly insightful in gaining a comprehensive understanding of the behaviour of both MLR and MRF models in the pre–deployment calibration dataset. It enabled the identification of the relationships between input features (O3, NO2, internal temperature, relative humidity) and the predicted outcomes. Additionally, the use of SHAP allowed for the diagnosis of potential issues, such as the non–parametric models' ability to extrapolate and predict pollution levels beyond the scope of the training calibration dataset (e.g., Nowack et al., 2021; Malings et al., 2019). These issues were confirmed through the validation process against ARPAT official reference.

As evident from Table 7, the MLR calibration model outperformed the MRF approach, showcasing a better transferability across diverse spatial and temporal settings. Besides, even though the pre–deployment dataset mainly represented a summer period, the physical patterns identified in the MLR model remained valid across seasons. Additionally, the SHAP heatmap (Fig. 6) provided insightful evidence of the O3 sensor's ability to handle the lower reading limit of the NO2 sensor for both AQs. This observation is important, especially in conditions with low NO2 concentrations, where the NO2 sensor's accuracy in providing readings might be compromised.

On the contrary, MRF did not align perfectly with the expected underlying physical model. Instead, it appeared to be "true to the data" due to its ability to memorize specific patterns from the pre–deployment dataset, as emerged by the SHAP analysis (Figure 6b). However, this characteristic posed challenges when trying to apply the model to unseen data, leading to

unsatisfactory performance in the field. This lack of generalization capability hindered the MRF model's effectiveness when faced with differing concentration regimes.

The seasonal analyses presented in Table 7 provided an overview of these seasonal changes in the stability and biases of AQ1 and AQ2 O3 and NO2 sensors for the application of the MLR calibration model after deployment. O3 pre–deployment calibration showed good performance in all seasons and for both stations the lowest nRMSE value was registered in summer 2018 and in summer 2019 and the highest value of nRMSE was recorded in winter 2018–2019. The decline in performance during the winter period was minimal, despite the fact that the pre–deployment calibration was mainly performed in the summer. Furthermore, the comparison of the summer period of 2018 and 2019 showed a decrease of 2% in nRMSE for both AQs and pollutants (O3 and NO2). The decrease in nRMSE for O3 was accompanied by an increase in the magnitude of MAE and MBE, pointing towards a possible linear drift in O3 sensor readings after a year of use. Conversely, for pre–deployment calibration of NO2, a decrease in MBE was observed. The decrease in MBE for NO2 and the prominent role of O3 raw readings and its negative impact on prediction, as identified through feature importance analysis of the pre–deployment MLR model, further reinforced the idea of a linear drift in O3 sensor readings. Similarly, the pattern of lowest and highest nRMSE values for O3 validation remained consistent also for the MRF model, being the lowest in the summer of 2018 and 2019 and the highest in the winter of 2018–2019 (Table S12). Notably, AQ1 outperforms AQ2 in both models; however, as mentioned earlier, the differences in nRMSE values between the MLR and MRF models were quite significant.

5   Conclusions and Perspective

In this study, the pre–deployment calibration and field validation of two low–cost (LC) stations named 'AIRQino,' developed by IBE–CNR in Florence (Italy), were addressed. The stations were equipped with O3 and NO2 MOS sensors, as well as meteorological sensors. Pre–deployment calibration was performed after developing and implementing a comprehensive calibration framework, consisting of several among parametric, non–parametric univariate and multiple algorithms, that allowed to identify the optimal calibration pathway. Ultimately, this resulted in robust LC performances outside the training conditions and the ability for easy adjustments to cope with changes in sensor performance over time. While selecting the most suitable LC calibration models, necessarily going beyond mere accuracy, this study primarily recommends to: (i) include multiple co-variates, such as internal (rather than external) temperature, relative humidity, and gaseous interference compounds, into the multiple regression models; (ii) analyze the importance of the features used in the multiple models to disclose their role when the calibrated LC stations are operated under field conditions rather than in a controlled environment.

As a novelty applied to LC MOS sensor calibration, the SHapley Additive exPlanations (SHAP) method was used to provide further insight into the role played by model individual predictors and their global and local impact on the overall LC sensor performances. This method was also used to hypothesize the model's capability to accurately describe conditions beyond the pre–deployment calibration period.

This study confirmed that machine learning models, such as MRF, can effectively calibrate LC sensors and mitigate the impact of environmental conditions and pollutant cross–sensitivity. However, while the MRF model demonstrated higher accuracy

than MLR during pre–deployment calibration, it faced challenges in accurately representing physical models and struggled to generalize on the field validation dataset. Furthermore, as well as being less computationally demanding and generally more suitable for non–experts, parametric models such as MLR have a defined equation that also includes a few parameters, which allows – when needed – easy adjustments for possible changes over time. Thus, drift correction or periodic automatable re–calibration operations can be readily scheduled, making parametric models advantageous. This aspect is particularly relevant for NO2 and O3 MOS sensors, as demonstrated in this study. Both sensors performed well with the same linear model form, requiring unique parameter values due to inter–sensor variability.

A limitation of the present work is that the LC stations have been calibrated during a period not particularly long (73 days) and a typically summer one, thus when pollution levels are generally meaningful for O3, but they are not for NO2 concentra–tions. Indeed, conducting a pre–deployment calibration during a winter period, when NO2 concentrations are typically higher, would be a valuable addition to the study. This step would provide a more comprehensive understanding of the AQs validation performance under varying pollution conditions and help address the limitation of the current calibration period biased towards summer data. Moreover, conducting a similar validation outside of Italy, in regions with differing pollution and meteorological conditions would be of great interest. For this purpose, in the ongoing activity, the AIRQino LC stations are planned to be deployed outside Italy, such as in Nice and Aix–en–Provence (France), Barcelona (Spain), Budapest (Hungary), Tirana (Alba–nia), and Niamey (Niger).

Furthermore, in the future, a new sensor for monitoring NO could hopefully be integrated into the LC stations and validated. As such, the combined monitoring of NO, NO2 and O3 concentrations and their daily and seasonal variability would allow a comprehensive pattern of the oxidant capacity of atmosphere, particularly effective in southern Mediterranean countries such as Italy (Pancholi et al., 2018). In addition, once the AQ VOC sensor will be validated, it will enable the monitoring of all O3 precursors (VOC and NOx). This comprehensive monitoring, combined with the application of SHapley Additive exPla–nations (SHAP) method, will lead to a full characterization of photochemical pollution in various areas of interest, including urban, sub–urban, or rural regions. Moreover, portability of LC sensors makes them ideal devices for filling knowledge gaps in regions that are difficult to access such as the open sea. Mounted on buoys or ships, for example, LC sensors could collect the high O3 levels that typically occur over these areas in summer due to high solar activity and rather low mixing height combined with a lack of O3–consuming NO emissions.

Appendix A

Table A1. Nomenclature

APD	Average partial dominance	**LC**	Low–cost	**RBF**	Radial basis function
AQ	AIRQino	**LNLR**	Logarithm regression	**RF**	Random Forest
CDLR	Cook's distance regression	**LR**	Linear regression	**RH**	Relative humidity
DA	Dominance Analysis	**MGB**	Multiple gradient boosting	**SHAP**	SHapley Additive exPlanations
EC	Electrochemical	**MLR**	Multiple linear regression	**SLR**	Supervised linear regression
EDA	Exploratory data analysis	**MOS**	Metal oxide sensors	**SNLR**	Supervised nonlinear regression
extT	External Temperature	**MRF**	Multiple random forest	**SVM**	Support vector machine
GB	Gradient Boosting	**PFI**	Permutation feature importance	**SVR**	Support vector regression
HBLR	Huber regression	**PLR2**	Polynomial regression of second degree	**TD**	Total dominance
ID	Individual dominance	**PLR3**	Polynomial regression of third degree	**VIF**	Variance impact factor
IntD	Interactional dominance	**PNLR**	Power nonlinear regression		
intT	Internal temperature	**PRI**	Percentage relative importance		

References

Aleixandre, M., Gerboles, M., and Spinelle, L.: Report of the laboratory and in-situ validation of micro-sensors and evaluation of suitability of model equations NO9: CairClipNO2 of CAIRPOL (F), Publications Office of the European Union, Luxembourg, oCLC: 1111194588, 2013.

Asair: Datasheet AM2305C, https://asairsensors.com/wp-content/uploads/2021/09/Data-Sheet-AM2315C-Humidity-and-Temperature-Module-ASAIR-V1.0.02.pdf.

Aula, K., Lagerspetz, E., Nurmi, P., and Tarkoma, S.: Evaluation of Low-Cost Air Quality Sensor Calibration Models, ACM Transactions on Sensor Networks, p. 3512889, https://doi.org/10.1145/3512889, 2022.

Azen, R. and Budescu, D. V.: The Dominance Analysis Approach for Comparing Predictors in Multiple Regression., Psychological Methods, 8, 129–148, https://doi.org/10.1037/1082-989X.8.2.129, 2003.

Barcelo-Ordinas, J. M., Ferrer-Cid, P., Garcia-Vidal, J., Ripoll, A., and Viana, M.: Distributed Multi-Scale Calibration of Low-Cost Ozone Sensors in Wireless Sensor Networks, Sensors, 19, 2503, https://doi.org/10.3390/s19112503, 2019.

Bart, M., Williams, D. E., Ainslie, B., McKendry, I., Salmond, J., Grange, S. K., Alavi-Shoshtari, M., Steyn, D., and Henshaw, G. S.: High Density Ozone Monitoring Using Gas Sensitive Semi-Conductor Sensors in the Lower Fraser Valley, British Columbia, Environmental Science & Technology, 48, 3970–3977, https://doi.org/10.1021/es404610t, 2014.

Bigi, A., Mueller, M., Grange, S. K., Ghermandi, G., and Hueglin, C.: Performance of NO, NO2 low cost sensors and three calibration approaches within a real world application, Atmospheric Measurement Techniques, 11, 3717–3735, https://doi.org/10.5194/amt-11-3717-2018, 2018.

Bisignano, A., Carotenuto, F., Zaldei, A., and Giovannini, L.: Field calibration of a low-cost sensors network to assess traffic-related air pollution along the Brenner highway, Atmospheric Environment, 275, 119 008, https://doi.org/10.1016/j.atmosenv.2022.119008, 2022.

Breiman, L.: Random Forests, Machine Learning, 45, 5–32, https://doi.org/10.1023/A:1010933404324, 2001.

Brilli, L., Carotenuto, F., Andreini, B. P., Cavaliere, A., Esposito, A., Gioli, B., Martelli, F., Stefanelli, M., Vagnoli, C., Venturi, S., Zaldei, A., and Gualtieri, G.: Low-Cost Air Quality Stations' Capability to Integrate Reference Stations in Particulate Matter Dynamics Assessment, Atmosphere, 12, 1065, https://doi.org/10.3390/atmos12081065, 2021.

Burgués, J. and Marco, S.: Low Power Operation of Temperature-Modulated Metal Oxide Semiconductor Gas Sensors, Sensors, 18, 339, https://doi.org/10.3390/s18020339, 2018.

Camalier, L., Cox, W., and Dolwick, P.: The effects of meteorology on ozone in urban areas and their use in assessing ozone trends, Atmospheric Environment, 41, 7127–7137, https://doi.org/10.1016/j.atmosenv.2007.04.061, 2007.

Cavaliere, A.: Code and dataset for: Development of Low-Cost Air Quality Stations for Next Generation Monitoring Networks: Calibration and Validation of NO2 and O3 Sensors, https://doi.org/10.5281/zenodo.7826791, 2023.

Cavaliere, A., Carotenuto, F., Di Gennaro, F., Gioli, B., Gualtieri, G., Martelli, F., Matese, A., Toscano, P., Vagnoli, C., and Zaldei, A.: Development of Low-Cost Air Quality Stations for Next Generation Monitoring Networks: Calibration and Validation of PM2.5 and PM10 Sensors, Sensors, 18, 2843, https://doi.org/10.3390/s18092843, 2018.

Chakraborty, S., Mittermaier, S., Carbonelli, C., and Servadei, L.: Explainable AI for Gas Sensors, in: 2022 IEEE Sensors, pp. 1–4, IEEE, https://doi.org/10.1109/SENSORS52175.2022.9967180, 2022.

Claveau, C., Giraudon, M., Coville, B., Saussac, A., Eymard, L., Turcati, L., and Payan, S.: Performance comparison between electrochemical and semiconductors sensors for the monitoring of O3, preprint, Gases/Laboratory Measurement/Validation and Intercomparisons, https://doi.org/10.5194/amt-2022-75, 2022.

425 Concas, F., Mineraud, J., Lagerspetz, E., Varjonen, S., Liu, X., Puolamäki, K., Nurmi, P., and Tarkoma, S.: Low-Cost Outdoor Air Quality Monitoring and Sensor Calibration: A Survey and Critical Analysis, ACM Transactions on Sensor Networks, 17, 1–44, https://doi.org/10.1145/3446005, 2021.

Cook, R. D.: Detection of Influential Observation in Linear Regression, Technometrics, 19, 15–18, https://doi.org/10.1080/00401706.1977.10489493, 1977.

430 Cordero, J. M., Borge, R., and Narros, A.: Using statistical methods to carry out in field calibrations of low cost air quality sensors, Sensors and Actuators B: Chemical, 267, 245–254, https://doi.org/10.1016/j.snb.2018.04.021, 2018.

De Vito, S., Piga, M., Martinotto, L., and Di Francia, G.: CO, NO2 and NOx urban pollution monitoring with on-field calibrated electronic nose by automatic bayesian regularization, Sensors and Actuators B: Chemical, 143, 182–191, https://doi.org/10.1016/j.snb.2009.08.041, 2009.

435 De Vito, S., Di Francia, G., Esposito, E., Ferlito, S., Formisano, F., and Massera, E.: Adaptive machine learning strategies for network calibration of IoT smart air quality monitoring devices, Pattern Recognition Letters, 136, 264–271, https://doi.org/10.1016/j.patrec.2020.04.032, 2020.

Dekking, F. M., Kraaikamp, C., Lopuhaä, H. P., and Meester, L. E.: A Modern Introduction to Probability and Statistics, Springer Texts in Statistics, Springer London, London, https://doi.org/10.1007/1-84628-168-7, 2005.

440 Di Lonardo, S., Zaldei, A., Toscano, P., Matese, A., Gioli, B., Rocchi, L., Vagnoli, C., De Filippis, T., Gualtieri, G., and Martelli, F.: The SensorWebBike for air quality monitoring in a smart city, in: IET Conference on Future Intelligent Cities, pp. 2 (4 .)–2 (4 .), Institution of Engineering and Technology, London, UK, https://doi.org/10.1049/ic.2014.0043, 2014.

Draper, N. R. and Smith, H.: Applied regression analysis, Wiley series in probability and statistics, Wiley, New York, 3rd ed edn., 1998.

Esposito, E., Salvato, M., Vito, S. D., Fattoruso, G., Castell, N., Karatzas, K., and Francia, G. D.: Assessing the Relocation Robustness of
445 on Field Calibrations for Air Quality Monitoring Devices, in: Sensors and Microsystems, edited by Leone, A., Forleo, A., Francioso, L., Capone, S., Siciliano, P., and Di Natale, C., vol. 457, pp. 303–312, Springer International Publishing, Cham, https://doi.org/10.1007/978-3-319-66802-4_38, series Title: Lecture Notes in Electrical Engineering, 2018.

Fine, G. F., Cavanagh, L. M., Afonja, A., and Binions, R.: Metal Oxide Semi-Conductor Gas Sensors in Environmental Monitoring, Sensors, 10, 5469–5502, https://doi.org/10.3390/s100605469, 2010.

450 Gu, K., Qiao, J., and Lin, W.: Recurrent Air Quality Predictor Based on Meteorology- and Pollution-Related Factors, IEEE Transactions on Industrial Informatics, 14, 3946–3955, https://doi.org/10.1109/TII.2018.2793950, 2018.

Gäbel, P., Koller, C., and Hertig, E.: Development of Air Quality Boxes Based on Low-Cost Sensor Technology for Ambient Air Quality Monitoring, Sensors, 22, 3830, https://doi.org/10.3390/s22103830, 2022.

Han, P., Mei, H., Liu, D., Zeng, N., Tang, X., Wang, Y., and Pan, Y.: Calibrations of Low-Cost Air Pollution Monitoring Sensors for CO,
455 NO2, O3, and SO2, Sensors, 21, 256, https://doi.org/10.3390/s21010256, 2021.

Han, S., Bian, H., Feng, Y., Liu, A., Li, X., Zeng, F., and Zhang, X.: Analysis of the Relationship between O3, NO and NO2 in Tianjin, China, Aerosol and Air Quality Research, 11, 128–139, https://doi.org/10.4209/aaqr.2010.07.0055, 2011.

Holstius, D. M., Pillarisetti, A., Smith, K. R., and Seto, E.: Field Calibrations of a Low-Cost Aerosol Sensor at a Regulatory Monitoring Site in California, Atmospheric Measurement Techniques, 7, 1121–1131, https://doi.org/10.5194/amt-7-1121-2014, 2014.

460 Idrees, Z. and Zheng, L.: Low cost air pollution monitoring systems: A review of protocols and enabling technologies, Journal of Industrial Information Integration, 17, 100 123, https://doi.org/10.1016/j.jii.2019.100123, 2020.

Johnson, N. E., Bonczak, B., and Kontokosta, C. E.: Using a gradient boosting model to improve the performance of low-cost aerosol monitors in a dense, heterogeneous urban environment, Atmospheric Environment, 184, 9–16, https://doi.org/10.1016/j.atmosenv.2018.04.019, 2018.

465 Karagulian, F.: New Challenges in Air Quality Measurements, in: Air Quality Networks, edited by De Vito, S., Karatzas, K., Bartonova, A., and Fattoruso, G., pp. 1–18, Springer International Publishing, Cham, https://doi.org/10.1007/978-3-031-08476-8_1, series Title: Environmental Informatics and Modeling, 2023.

Karagulian, F., Barbiere, M., Kotsev, A., Spinelle, L., Gerboles, M., Lagler, F., Redon, N., Crunaire, S., and Borowiak, A.: Review of the Performance of Low-Cost Sensors for Air Quality Monitoring, Atmosphere, 10, 506, https://doi.org/10.3390/atmos10090506, 2019.

470 Lin, Y., Dong, W., and Chen, Y.: Calibrating Low-Cost Sensors by a Two-Phase Learning Approach for Urban Air Quality Measurement, Proceedings of the ACM on Interactive, Mobile, Wearable and Ubiquitous Technologies, 2, 1–18, https://doi.org/10.1145/3191750, 2018.

Lundberg, S. and Lee, S.-I.: A Unified Approach to Interpreting Model Predictions, Advances in neural information processing systems, https://doi.org/10.48550/ARXIV.1705.07874, publisher: arXiv Version Number: 2, 2017.

Lundberg, S. and Lee, S.-I.: SHAP, https://shap.readthedocs.io/en/latest/, 2022.

475 Maag, B., Saukh, O., Hasenfratz, D., and Thiele, L.: Pre-Deployment Testing, Augmentation and Calibration of Cross-Sensitive Sensors., in: EWSN, pp. 169–180, 2016.

Maag, B., Zhou, Z., and Thiele, L.: A Survey on Sensor Calibration in Air Pollution Monitoring Deployments, IEEE Internet of Things Journal, 5, 4857–4870, https://doi.org/10.1109/JIOT.2018.2853660, conference Name: IEEE Internet of Things Journal, 2018.

Malings, C., Tanzer, R., Hauryliuk, A., Kumar, S. P. N., Zimmerman, N., Kara, L. B., Presto, A. A., and R. Subramanian: Development
480 of a general calibration model and long-term performance evaluation of low-cost sensors for air pollutant gas monitoring, Atmospheric Measurement Techniques, 12, 903–920, https://doi.org/10.5194/amt-12-903-2019, 2019.

Masson, N., Piedrahita, R., and Hannigan, M.: Approach for quantification of metal oxide type semiconductor gas sensors used for ambient air quality monitoring, Sensors and Actuators B: Chemical, 208, 339–345, https://doi.org/10.1016/j.snb.2014.11.032, 2015.

Maxim Integrated: Datasheet DS18B20.

485 Mead, M., Popoola, O., Stewart, G., Landshoff, P., Calleja, M., Hayes, M., Baldovi, J., McLeod, M., Hodgson, T., Dicks, J., Lewis, A., Cohen, J., Baron, R., Saffell, J., and Jones, R.: The use of electrochemical sensors for monitoring urban air quality in low-cost, high-density networks, Atmospheric Environment, 70, 186–203, https://doi.org/10.1016/j.atmosenv.2012.11.060, 2013.

Meng, X., Liu, C., Chen, R., Sera, F., Vicedo-Cabrera, A. M., Milojevic, A., Guo, Y., Tong, S., Coelho, M. d. S. Z. S., Saldiva, P. H. N., et al.: Short Term Associations of Ambient Nitrogen Dioxide with Daily Total, Cardiovascular, and Respiratory Mortality: Multilocation
490 Analysis in 398 Cities, BMJ, p. n534, https://doi.org/10.1136/bmj.n534, 2021.

Miech, J., Stanton, L., Gao, M., Micalizzi, P., Uebelherr, J., Herckes, P., and Fraser, M.: Calibration of Low-Cost NO2 Sensors through Environmental Factor Correction, Toxics, 9, 281, https://doi.org/10.3390/toxics9110281, 2021.

Mijling, B., Jiang, Q., de Jonge, D., and Bocconi, S.: Field calibration of electrochemical NO2 sensors in a citizen science context, Atmospheric Measurement Techniques, 11, 1297–1312, https://doi.org/10.5194/amt-11-1297-2018, 2018.

495 Morawska, L., Thai, P. K., Liu, X., Asumadu-Sakyi, A., Ayoko, G., Bartonova, A., Bedini, A., Chai, F., Christensen, B., Dunbabin, M., Gao, J., Hagler, G. S., Jayaratne, R., Kumar, P., Lau, A. K., Louie, P. K., Mazaheri, M., Ning, Z., Motta, N., Mullins, B., Rahman, M. M., Ristovski, Z., Shafiei, M., Tjondronegoro, D., Westerdahl, D., and Williams, R.: Applications of low-cost sensing tech-

nologies for air quality monitoring and exposure assessment: How far have they gone?, Environment International, 116, 286–299, https://doi.org/10.1016/j.envint.2018.04.018, 2018.

500   Mueller, M., Meyer, J., and Hueglin, C.: Design of an ozone and nitrogen dioxide sensor unit and its long-term operation within a sensor network in the city of Zurich, Atmospheric Measurement Techniques, 10, 3783–3799, https://doi.org/10.5194/amt-10-3783-2017, 2017.

Narayana, M. V., Jalihal, D., and Nagendra, S. M. S.: Establishing A Sustainable Low-Cost Air Quality Monitoring Setup: A Survey of the State-of-the-Art, Sensors, 22, 394, https://doi.org/10.3390/s22010394, 2022.

Nowack, P., Konstantinovskiy, L., Gardiner, H., and Cant, J.: Machine learning calibration of low-cost NO2 and PM10 sensors: non-linear 505   algorithms and their impact on site transferability, Atmospheric Measurement Techniques, 14, 5637–5655, https://doi.org/10.5194/amt-14-5637-2021, 2021.

Nuvolone, D., Petri, D., and Voller, F.: The Effects of Ozone on Human Health, Environmental Science and Pollution Research, 25, 8074–8088, https://doi.org/10.1007/s11356-017-9239-3, 2018.

Pancholi, P., Kumar, A., Bikundia, D. S., and Chourasiya, S.: An observation of seasonal and diurnal behavior of O3–NOx relationships and 510   local/regional oxidant (OX= O3+ NO2) levels at a semi-arid urban site of western India, Sustainable Environment Research, 28, 79–89, https://doi.org/10.1016/j.serj.2017.11.001, 2018.

Pedregosa, F., Varoquaux, G., Gramfort, A., Michel, V., Thirion, B., Grisel, O., Blondel, M., Prettenhofer, P., Weiss, R., Dubourg, V., Vanderplas, J., Passos, A., and Cournapeau, D.: Scikit-learn: Machine Learning in Python, Journal of Machine Learning Research, 12, 2825–2830, 2011.

515   Peterson, P., Aujla, A., Grant, K., Brundle, A., Thompson, M., Vande Hey, J., and Leigh, R.: Practical Use of Metal Oxide Semiconductor Gas Sensors for Measuring Nitrogen Dioxide and Ozone in Urban Environments, Sensors, 17, 1653, https://doi.org/10.3390/s17071653, 2017.

Piedrahita, R., Xiang, Y., Masson, N., Ortega, J., Collier, A., Jiang, Y., Li, K., Dick, R. P., Lv, Q., Hannigan, M., and Shang, L.: The next generation of low-cost personal air quality sensors for quantitative exposure monitoring, Atmospheric Measurement Techniques, 7, 520   3325–3336, https://doi.org/10.5194/amt-7-3325-2014, 2014.

Rai, A. C., Kumar, P., Pilla, F., Skouloudis, A. N., Di Sabatino, S., Ratti, C., Yasar, A., and Rickerby, D.: End-user perspective of low-cost sensors for outdoor air pollution monitoring, Science of The Total Environment, 607-608, 691–705, https://doi.org/10.1016/j.scitotenv.2017.06.266, 2017.

Sahu, R., Nagal, A., Dixit, K. K., Unnibhavi, H., Mantravadi, S., Nair, S., Simmhan, Y., Mishra, B., Zele, R., Sutaria, R., Motghare, 525   V. M., Kar, P., and Tripathi, S. N.: Robust statistical calibration and characterization of portable low-cost air quality monitoring sensors to quantify real-time O3 and NO2 concentrations in diverse environments, Atmospheric Measurement Techniques, 14, 37–52, https://doi.org/10.5194/amt-14-37-2021, 2021.

Sales-Lérida, D., Bello, A. J., Sánchez-Alzola, A., and Martínez-Jiménez, P. M.: An Approximation for Metal-Oxide Sensor Calibration for Air Quality Monitoring Using Multivariable Statistical Analysis, Sensors, 21, 4781, https://doi.org/10.3390/s21144781, 2021.

530   Sayahi, T., Garff, A., Quah, T., Lê, K., Becnel, T., Powell, K. M., Gaillardon, P.-E., Butterfield, A. E., and Kelly, K. E.: Long-term calibration models to estimate ozone concentrations with a metal oxide sensor, Environmental Pollution, 267, 115 363, https://doi.org/10.1016/j.envpol.2020.115363, 2020.

Schmitz, S., Towers, S., Villena, G., Caseiro, A., Wegener, R., Klemp, D., Langer, I., Meier, F., and Von Schneidemesser, E.: Unravelling a Black Box: An Open-Source Methodology for the Field Calibration of Small Air Quality Sensors, Atmospheric Measurement Techniques, 535   14, 7221–7241, https://doi.org/10.5194/amt-14-7221-2021, 2021.

Seabold, S. and Perktold, J.: statsmodels: Econometric and statistical modeling with python, in: 9th Python in Science Conference, 2010.

Sensortech, S. G. X.: Datasheet MiCS-2714, https://www.sgxsensortech.com/content/uploads/2014/08/1107_Datasheet-MiCS-2714.pdf, a.

Sensortech, S. G. X.: Datasheet MiCS-2614, https://sensorsandpower.angst-pfister.com/fileadmin/products/datasheets/188/MOS-Ozone-MiCS-2614_1620-21530-0006-E-0714.pdf, b.

540 Shekhar, S., Bhagat, S., and K., S.: Dominance-Analysis, https://github.com/dominance-analysis/dominance-analysis, 2019.

Smets, K., Verdonk, B., and Jordaan, E. M.: Evaluation of performance measures for SVR hyperparameter selection, in: 2007 International Joint Conference on Neural Networks, pp. 637–642, IEEE, 2007.

Spiess, A.-N. and Neumeyer, N.: An evaluation of R2 as an inadequate measure for nonlinear models in pharmacological and biochemical research: a Monte Carlo approach, BMC Pharmacology, 10, 6, https://doi.org/10.1186/1471-2210-10-6, 2010.

545 Spinelle, L., Aleixandre, M., Gerboles, M., et al.: Protocol of evaluation and calibration of low-cost gas sensors for the monitoring of air pollution, Publications Office of the European Union: Luxembourg, https://doi.org/10.2788/9916, 2013.

Spinelle, L., Gerboles, M., Villani, M. G., Aleixandre, M., and Bonavitacola, F.: Field calibration of a cluster of low-cost available sensors for air quality monitoring. Part A: Ozone and nitrogen dioxide, Sensors and Actuators B: Chemical, 215, 249–257, https://doi.org/10.1016/j.snb.2015.03.031, 2015.

550 Spinelle, L., Gerboles, M., Aleixandre, M., and Bonavitacola, F.: Evaluation of metal oxides sensors for the monitoring of o3 in ambient air at ppb level, Chemical Engineering Transactions, 54, 319–324, https://doi.org/10.3303/CET1654054, 2016.

Spinelle, L., Gerboles, M., Villani, M. G., Aleixandre, M., and Bonavitacola, F.: Field calibration of a cluster of low-cost commercially available sensors for air quality monitoring. Part B: NO, CO and CO2, Sensors and Actuators B: Chemical, 238, 706–715, https://doi.org/10.1016/j.snb.2016.07.036, 2017.

555 TeamHG-Memex: Eli5, https://eli5.readthedocs.io/en/latest/, 2022.

Vega García, M. and Aznarte, J. L.: Shapley additive explanations for NO2 forecasting, Ecological Informatics, 56, 101 039, https://doi.org/10.1016/j.ecoinf.2019.101039, 2020.

Wang, A., Machida, Y., deSouza, P., Mora, S., Duhl, T., Hudda, N., Durant, J. L., Duarte, F., and Ratti, C.: Leveraging Machine Learning Algorithms to Advance Low-Cost Air Sensor Calibration in Stationary and Mobile Settings, Atmospheric Environment, 301, 119 692, https://doi.org/10.1016/j.atmosenv.2023.119692, 2023.

560 Wang, C., Yin, L., Zhang, L., Xiang, D., and Gao, R.: Metal Oxide Gas Sensors: Sensitivity and Influencing Factors, Sensors, 10, 2088–2106, https://doi.org/10.3390/s100302088, number: 3 Publisher: Molecular Diversity Preservation International, 2010.

Wei, P., Ning, Z., Ye, S., Sun, L., Yang, F., Wong, K., Westerdahl, D., and Louie, P.: Impact Analysis of Temperature and Humidity Conditions on Electrochemical Sensor Response in Ambient Air Quality Monitoring, Sensors, 18, 59, https://doi.org/10.3390/s18020059, 2018.

565 Williams, D. E., Henshaw, G. S., Bart, M., Laing, G., Wagner, J., Naisbitt, S., and Salmond, J. A.: Validation of low-cost ozone measurement instruments suitable for use in an air-quality monitoring network, Measurement Science and Technology, 24, 065 803, https://doi.org/10.1088/0957-0233/24/6/065803, 2013.

World Health Organization: WHO global air quality guidelines: particulate matter (PM2.5 and PM10), ozone, nitrogen dioxide, sulfur dioxide and carbon monoxide, World Health Organization, Geneva, https://apps.who.int/iris/handle/10665/345329, section: xxi, 273 p., 2021.

570 Yang, J.: Fast TreeSHAP: Accelerating SHAP Value Computation for Trees, https://doi.org/10.48550/ARXIV.2109.09847, publisher: arXiv Version Number: 3, 2021.

Yang, J.: FastTreeSHAP, https://github.com/linkedin/FastTreeSHAP, 2022.

Zaldei, A., Camilli, F., De Filippis, T., Di Gennaro, F., Di Lonardo, S., Dini, F., Gioli, B., Gualtieri, G., Matese, A., Nunziati, W., Rocchi, L., Toscano, P., and Vagnoli, C.: An integrated low-cost road traffic and air pollution monitoring platform for next citizen observatories, Transportation Research Procedia, 24, 531–538, https://doi.org/10.1016/j.trpro.2017.06.002, 2017.

Zauli-Sajani, S., Marchesi, S., Pironi, C., Barbieri, C., Poluzzi, V., and Colacci, A.: Assessment of air quality sensor system performance after relocation, Atmospheric Pollution Research, 12, 282–291, https://doi.org/10.1016/j.apr.2020.11.010, 2021.

Zimmerman, N., Presto, A. A., Kumar, S. P. N., Gu, J., Hauryliuk, A., Robinson, E. S., Robinson, A. L., and R. Subramanian: A machine learning calibration model using random forests to improve sensor performance for lower-cost air quality monitoring, Atmospheric Measurement Techniques, 11, 291–313, https://doi.org/10.5194/amt-11-291-2018, 2018.